REV7/FANCV Binds to CAMP and Promotes Homologous Recombination Repair

Feng Li
Dana-Farber Cancer Institute
Prabha Sarangi
Dana-Farber Cancer Institute
Hanrong Feng
Dana-Farber Cancer Institute
Lisa Moreau
Dana-Farber Cancer Institute
Huy Nguyen
Dana-Farber Cancer Institute
Connor Clairmont
Dana-Farber Cancer Institute
Alan D'Andrea (alan_dandrea@dfci.harvard.edu)
Dana-Farber Cancer Institute https://orcid.org/0000-0001-6168-6294

Biological Sciences - Article

Keywords: REV7, TRIP13, CAMP, Homologous Recombination, Fanconi Anemia

Posted Date: August 12th, 2021

DOI: https://doi.org/10.21203/rs.3.rs-757230/v1

REV7/FANCV Binds to CAMP and Promotes Homologous Recombination Repair

Feng Li, Prabha Sarangi, Hanrong Feng, Lisa Moreau, Huy Nguyen, Connor Clairmont, Alan D. D'Andrea

1. Department of Radiation Oncology, Dana-Farber Cancer Institute, Boston, MA, 02215, USA
2. Center for DNA Damage and Repair, Dana-Farber Cancer Institute, Boston, MA, 02215, USA

Corresponding Author:

Alan D. D'Andrea, M.D.
Director: Center for DNA Damage and Repair
The Fuller-American Cancer Society Professor
Harvard Medical School
Chief, Division of Genomic Stability and DNA Repair
Department of Radiation Oncology
Dana-Farber Cancer Institute, HIM 243
450 Brookline Ave.
Boston, MA 02215
617-632-2080
FAX: 617-632-6069
Alan_Dandrea@dfci.harvard.edu

Running Title: REV7/CAMP promotes Homologous Recombination

Keywords: REV7, TRIP13, CAMP, Homologous Recombination, Fanconi Anemia

A critical determinant of DNA repair pathway choice is the HORMA protein REV7, a small abundant adaptor which binds to various DNA repair proteins through its C-terminal seatbelt domain [1,2]. The REV7 seatbelt binds to the REV3 polymerase to form the Polymerase ζ complex, a positive regulator of translesion synthesis (TLS) repair [3]. Alternatively, the REV7 seatbelt binds to SHLD3 in the Shieldin complex, a positive regulator of NHEJ repair [4-8]. Recent studies have identified another novel REV7 seatbelt-binding protein, CAMP (Chromosome Alignment-Maintaining Phosphoprotein) [9,10], though its role in DNA repair is unknown. Here, we show that the REV7-CAMP complex promotes homologous recombination (HR) repair by sequestering REV7 from the Shieldin complex. CAMP competes directly with the SHLD3 subunit of the Shieldin complex for a limited pool of C-REV7, thereby inhibiting the REV7-mediated recruitment of the SHLD2 and SHLD1 effector subunits to DNA double strand breaks. CAMP thereby channels DNA repair away from error-prone NHEJ and towards the competing error-free HR pathway. Similarly, CAMP competes with the REV3 component of the POLζ complex, thereby reducing the level of mutagenic TLS repair. CAMP has a distinct function in promoting chromosome alignment which is independent of its REV7 binding activity. Importantly, in human tumors, CAMP overexpression promotes HR, confers PARP inhibitor resistance, and correlates with poor prognosis. Thus, by binding to either REV3, SHLD3, or CAMP through its seatbelt, the REV7 protein can promote either TLS repair, NHEJ repair, or HR repair respectively.

REV7 (also known as MAD2L2, MAD2B, or FANCV), is a highly-conserved member of the HORMA family of proteins, named for its three founding members: HOp1, a meiotic chromosome axis factor, REV7, and MAD2, a spindle assembly checkpoint protein [1,2]. REV7 adopts the two classic closed and open seatbelt conformations of HORMA proteins, and SHLD3 and REV3 are among its seatbelt dependent binding partners. The AAA+ ATPase, TRIP13, along with its substrate adaptor p31^{comet}, can open REV7 and release SHLD3 or REV3 [11,12]. The mechanism by which REV7 is converted from the inactive open conformation back to the active closed form is less well understood, and it may involve either the binding of another, unknown SBM-containing protein or new post-translational modifications.

REV7 has at least one other demonstrated seatbelt-binding partner, CAMP (also known as C13orf80, CHAMP1, or ZNF828). CAMP is a little-known but highly conserved zinc finger protein first identified as a REV7 interactor [10]. CAMP localizes to chromosomes, recruits REV7 to spindles, and plays a role in kinetochore-microtubule interactions. Disruption of CAMP leads to characteristic defects in chromosome alignment in mitosis. Germline heterozygous mutations in CAMP are associated with a rare syndromic form of intellectual disability in humans [13]. Crystallographic analysis of the REV7/CAMP complex [9] revealed a strong similarity to the REV7/REV3 interaction surface [3]. Despite the clear role of REV7 in DNA repair pathway choice, little is known about the role of its interactor CAMP in DNA repair.

REV7/CAMP Complex promotes Homologous Recombination Repair

In order to determine the possible involvement of CAMP in DNA repair, we knocked down CAMP expression with siRNA in U2OS cells (**Figure 1**). Interestingly, CAMP knockdown resulted in a reduction in HR activity, based on the decrease in GFP fluorescence generated by the

DR-GFP template versus the EJ5-GFP template [14,15] (**Fig. 1a, b** and **Extended Data Fig. 1a**). Since an early step in HR repair is double strand break (DSB) end resection [16], we used the SMART assay [17] to quantify resection. Indeed, two siRNAs to CAMP decreased DSB end-resection (**Fig. 1c**). Cells with an HR deficiency have a defect in RAD51 foci assembly and exhibit sensitivity to PARP inhibitors [18,19]. Accordingly, RPE-1 cells or U2OS cells with a CRISPR-Cas9-mediated knockout of CAMP exhibited reduced RAD51 foci (**Fig. 1d**) and were sensitive to the PARP inhibitor, olaparib (**Fig. 1e, f** and **Extended Data Fig. 1b-d**). Previous studies have demonstrated that CAMP interacts directly with REV7 [9], a known regulator of DNA HR repair [20,21]. To confirm and extend these findings, we showed that DNA damage with UV radiation activates the binding of CAMP and REV7 and stimulates the colocalization of REV7 and CAMP in nuclear foci (**Extended Data Fig. 1e-g**). Moreover, CAMP promotes the chromatin localization of REV7 (**Extended Data Fig. 1h, i).** Taken together, we reasoned that the DNA damage inducible interaction of CAMP and REV7 might be required for HR repair.

DNA damage activates REV7 seatbelt closure and partner protein binding

We next determined the mechanism by which DNA damage activates the closing of the REV7 seatbelt (**Figure 2**). REV7 has a single, highly-conserved TQ site (T103) which is a possible site of DNA damage-inducible, ATM-dependent phosphorylation (**Extended Data Fig. 2a**) [22]. Interestingly, this TQ site aligns with a negatively-charged amino acid (E105) in the primary sequence of another HORMA protein, MAD2. Moreover, in the closed conformation of MAD2, an electrostatic interaction between E105 and the positively-charged K192, likely contributes to the closing of the MAD2 seatbelt (**Extended Data Fig. 2b**). Similarly, REV7 has a K198 residue at the corresponding site. We therefore reasoned that a DNA-damage inducible, ATM-dependent,

115 phosphorylation of T103 of REV7 could account, at least in part, for the DNA-damage inducible
116 closing of REV7 and the binding of proteins with a SBM, such as SHLD3, REV3, and CAMP.
117 To test this hypothesis, we initially determined whether DNA damage activates the
118 phosphorylation of REV7 at T103, using an anti-p(S/T)Q antibody (**Extended Data Fig. 2c**).
119 Indeed, DNA damage activated the phosphorylation of REV7, and a point mutation of REV7
120 (T103A) reduced this UV-activated phosphorylation of REV7 *in vitro* **(Fig. 2a***)* and its chromatin
121 recruitment (**Fig. 2b**)**.** Consistent with this, an ATM inhibitor reduced the DNA damage-
122 dependent phosphorylation of REV7, reduced the chromatin recruitment of REV7, and decreased
123 the assembly of REV7 foci (**Fig. 2c, d** and **Extended Data Fig. 2d, e**). Similarly, UV damage
124 failed to activate the assembly of nuclear foci of the REV7-T103A mutant protein, confirming that
125 REV7 closing correlates with nuclear foci formation (**Extended Data Fig. 2f**). Unlike wild-type
126 REV7, the REV7-T103A mutant protein failed to reduce RAD51 foci (**Extended Data Fig. 2g, h**)
127 and failed to restore PARP inhibitor sensitivity in REV7(-/-) cells (**Extended Data Fig. 2i, j**).
128 Moreover, knockdown of TRIP13 or p31 resulted in increased binding of CAMP to REV7, while
129 overexpression of TRIP13 reduced this interaction, similarly to our previous findings with the
130 other seatbelt interactors SHLD3 and REV3 (**Fig. 2e, f**). The REV7-T103A mutant exhibited
131 reduced binding to either SHLD3, CAMP, or REV3 (**Fig. 2g-i**). Taken together, DNA damage
132 activates the ATM-dependent phosphorylation of T103 on REV7, thereby promoting the closing
133 of the REV7 seatbelt and the binding of SBM proteins, such as SHLD3 and CAMP. The
134 TRIP13/p31 complex opens REV7 and releases these binding partners.
135
136 **CAMP increases HR activity by competing with SHLD3 for binding to REV7**

REV7 is an abundant cellular protein, and it has several known binding partners [8]. Some of these binding partners bind to the C-terminal seatbelt domain of REV7, including SHLD3, REV3, and CAMP [1,2]. We reasoned that these partners might compete for seatbelt binding under different cellular conditions or cell cycle stages. The REV7 seatbelt binding protein, SHLD3, promotes the assembly of the Shieldin Complex [4-6,8], thereby blocking the resection of DSBs, recruiting the CST/Polα complex [7], and promoting blunt end ligation via the NHEJ pathway. The TRIP13 ATPase, along with its binding partner p31^{comet}, opens the seatbelt of REV7 and releases SHLD3 [11,12].

As CAMP is much more abundant in cells than SHLD3, we determined whether CAMP regulates REV7 binding to SHLD3 (**Figure 3**). In HEK293T cells, GFP-SHLD3 binds to REV7, and siRNA knockdown of CAMP resulted in increased co-immunoprecipitation of these proteins, demonstrating that CAMP functions as a negative regulator of the Shieldin complex (**Fig. 3a**). The REV7 seatbelt also binds to REV3, and the REV7/REV3 (POLζ) complex promotes error-prone Translesion DNA Synthesis (TLS) and enhanced point mutagenesis. We reasoned that CAMP might also sequester REV7 from the REV7/REV3 complex and reduce error-prone TLS activity. To test this hypothesis, we generated and expressed a GFP fusion protein containing the seatbelt binding domain of REV3. As predicted, knocking out CAMP resulted in an increased binding of the TLS polymerase subunit REV3 to REV7 in U2OS cells (**Fig. 3b**). Consistent with this result, CRISPR-Cas9-mediated knockout of CAMP in U2OS cells or RPE-1 cells resulted in increased REV7/REV3 activity, as measured by MMC resistance and reduced MMC-induced chromosome radials (**Fig. 3c-e** and **Extended Data Fig. 3a, b**). The TRIP13/p31 complex promotes the ATP-dependent opening of the REV7/SHLD3 complex and releases SHLD3 [11]. Taken together, these

159 results support a mechanism in which CAMP promotes DSB end resection by sequestering REV7
160 from SHLD3 and preventing the assembly of the Shieldin complex.
161
162 **The REV7 binding activity of CAMP is required for HR repair but not for correction of**
163 **chromosome misalignment**
164 In its primary sequence, CAMP has non-overlapping N-ZNF, SPE (aa143–290), WK
165 (aa291–478), FPE, and C-ZNF regions (**Fig. 4a**). While the CAMP-WK region is required for
166 REV7 binding and recruitment of REV7 to spindles, the CAMP-FPE region appears to play an
167 independent role in chromosome alignment [10]. To confirm and extend these results, we
168 generated two mutant forms of CAMP. According to the molecular structure of the
169 REV7/CAMP complex [9], the WKPAKPAPS - motif of CAMP, corresponding to the known
170 consensus of a REV7 Seatbelt Binding Motif (SBM), interacts directly with the seatbelt domain
171 of REV7 (**Fig. 4b**), albeit with distinct amino acid residue interactions compared to the
172 REV7/REV3 or the REV7/SHLD3 interactions. We therefore generated a mutant form of
173 CAMP which is predicted to disrupt this REV7 binding interaction (ie, the W334A/K335A
174 double mutation, referred to as the CAMP-2A mutation). We also generated an in-frame
175 deletion in CAMP (del-FPE CAMP), previously shown to be defective in the rescue of
176 chromosome abnormalities in CAMP-/- cells [10].
177 As predicted, when expressed in RPE1 CAMP-/- cells, the CAMP-2A mutant failed to
178 bind to REV7, while the del-FPE CAMP mutant was competent for REV7 binding (**Fig. 4c**).
179 Indeed, the CAMP-2A mutant failed to correct the PARPi sensitivity of in CAMP-/- cells, further
180 confirming that REV7 binding and sequestration by CAMP is required for enhancement of HR
181 activity (**Fig. 4d**). The failure of CAMP-2A to restore PARP inhibitor resistance and to reduce

MMC sensitivity was confirmed in the U2OS wild-type or CAMP-/- cells (**Extended Data Fig. 4c-g**). Interestingly, complementation with the CAMP del-FPE mutant yielded PARPi resistance, indicating that the FPE domain is not required for enhancement of HR activity.

We next evaluated these two mutant proteins for their ability to correct chromosome misalignment in CAMP-/- cells. Consistent with a previous report [10], CRISPR-knockout of CAMP in RPE1 cells results in a severe defect in chromosome alignment (**Extended Data Fig. 4a, b**). The CAMP del-FPE mutant protein failed to complement the chromosome misalignment and the G2/M accumulation of the CAMP-/- cells, but the WT CAMP protein or the CAMP-2A mutant were functional in these assays (**Fig. 4e, f**). Taken together, the WK and FPE domains of CAMP have independent, non-overlapping functions. Moreover, REV7 binding to CAMP is required for HR activity; however, the CAMP-mediated recruitment of REV7 to the spindle is not required for the correction of chromosome alignment.

CAMP regulates homologous recombination through REV7

CAMP regulates HR activity through its ability to sequester REV7 from the Shieldin complex. Thus, we expect that eliminating CAMP in cells already lacking REV7 should not affect HR (**Figure 5).** HR activity was scored by measuring the level of RAD51 and pRPA foci, both known to be increased in the setting of HR. As predicted siRNA knockdown of CAMP in wild-type RPE1 cells resulted in reduced HR activity but failed to reduce HR activity in cells in which REV7 was knocked out **(Fig. 5a, b** and **Extended Data Fig. 5a, b**). The REV7-/- cells exhibited increased HR activity, as measured by their PARP inhibitor resistance (**Fig. 5c**), regardless of their CAMP expression level. Consistent with these results, knockdown of CAMP in a SHLD2-deficient cell line, HCC1937, failed to cause Olaparib sensitivity **(Extended Data**

Fig. 5c). Taken together, the ability of CAMP to enhance HR is directly dependent on the presence of the REV7 protein.

We next sought additional evidence that CAMP upregulation correlates with PARP inhibitor resistance. We used a panel of BRCA1-deficient cell lines with acquired PARPi-resistance, collected through serial selection in increasing concentrations of PARPi (**Extended Data Fig. 5d**) [23]. These cells exhibited multiple independent mechanisms of PARPi resistance, including downregulation of the Shieldin Complex or upregulation of ATR/CHK1 pathway activity [23]. Interestingly, one of these PARPi-resistant clones (NA5) exhibited high CAMP mRNA expression compared to the parental PARPi-sensitive cell line (**Extended Data Fig. 5e**). Knockdown of CAMP in these cells restored PARPi sensitivity (**Fig. 5d**). In contrast, knockdown of CAMP in another line (NA1), which has a relatively normal level of CAMP but has a lower level of REV7 expression compared to the parental line, had no effect on PARPi sensitivity. Taken together, *BRCA1*-deficient cells can acquire PARPi resistance, at least in part, by upregulating CAMP expression.

To further validate this model, we next sought clinical evidence that CAMP expression might affect cancer patient survival. We reasoned that human tumors with an underlying defect in an HR pathway might upregulate CAMP as a compensatory mechanism to tolerate their low HR and their replication stress. To test this hypothesis, we correlated the level of CAMP expression in ovarian tumors with patient survival. For patients with tumors with low REV7 expression, the level of expression of CAMP did not affect survival (**Fig. 5e).** Thus, consistent with our cellular data, the elevated HR activity in cells with low or absent REV7 expression was unaffected by CAMP expression levels. Interestingly, for patients with tumors with high REV7 expression, the level of CAMP expression significantly affected patient survival. As predicted,

the high CAMP expression correlated with a more aggressive tumor and poor patient prognosis, perhaps resulting from the improved HR activity in these tumors. Consistent with these observations, in cancer cell lines the level of CAMP mRNA expression strongly correlates with the level of CCNE1 mRNA expression (**Fig. 5f**), suggesting cancer cells with a high degree of replication stress, resulting from CCNE1 amplification, may rely on CAMP-mediated HR for their survival. Indeed, breast cancer cell lines with high expression of CCNE1 mRNA are more dependent on CAMP for their proliferation and survival (**Fig. 5g**). Interestingly, CAMP expression is also upregulated in BRCA1-deficient and BRCA2-deficient tumors, and this correlates with poor patient prognosis (**Extended Data Fig. 5f-h**).

We conclude that REV7, through its C-terminal seatbelt, can bind to three different factors, SHLD3, REV3, and CAMP, to elicit distinct repair outcomes. The REV7-SHLD3 interaction mediates the assembly and accrual of the Shieldin complex at DSBs to block end resection and channel repair through NHEJ. The REV7-REV3 interaction promotes Polζ Translesion Synthesis (TLS) complex through its interaction with REV1 and bypasses bulky adducts on DNA during replication, thereby promoting mutagenesis. The REV7-CAMP complex, by sequestering REV7 from REV7-SHLD3 and REV7-REV3 complexes, can promote error-free HR repair and function as a negative regulator of the error-prone NHEJ and TLS repair pathways, respectively.

CAMP is also a subunit of a large multisubunit complex of HP1α heterochromatin binding proteins. This complex includes HP1α, POGZ, LEDGF, and HDGFRP2 [11,24-27]. REV7 coimmunoprecipitates with multiple components of this complex [8], further suggesting a functional connection with DNA repair regulation. Interestingly, knockdown or knockout of any of the subunits of this complex, such as HP1α [28], LEDGF [25] or HDGFRP2 [24], similar to the

knockdown of CAMP, reduces DSB end resection and HR (**Figure 3E**) and PARP inhibitor sensitivity [29]. Taken together, these results suggest that this CAMP-containing multisubunit complex may have a functional role in sequestering REV7, preventing its association with SHLD3 in the Shieldin complex, and promoting HR repair locally in heterochromatin.

ACKNOWLEDGMENTS

We thank all members of the D'Andrea laboratory for their helpful suggestions and comments. This work was supported by grants from the US National Institutes of Health (R37HL052725 and P01HL048546), the US Department of Defense (BM110181), the Breast Cancer Research Foundation, the Fanconi Anemia Research Fund, the Ludwig Center at Harvard, and the Smith Family Foundation (to A.D.D.) and the Claudia Adams Barr Program in Innovative Basic Cancer Research (to F.L. and P.S).

AUTHOR CONTRIBUTIONS

F.L., C.C., P.S., and A.D.D. conceived the study, analyzed the data, and wrote the manuscript. H.F., L.M, and H.N. performed experiments and analyzed the data.

DISCLOSURES

A.D. D'Andrea is a consultant/advisory board member for Lilly Oncology, Merck-EMD Serono, Cyteir Therapeutics, Third Rock Ventures, AstraZeneca, Ideaya Inc., Cedilla Therapeutics Inc., a stockholder in Ideaya Inc., Cedilla Therapeutics Inc., and Cyteir, and reports receiving commercial research grants from Lilly Oncology and Merck-EMD Serono.

FIGURE LEGENDS

Figure 1. CAMP promotes homologous recombination

a, Graph showing the percentage of GFP-positive cells after DR-GFP analysis. U2OS cells were infected with I-SceI adenovirus and knocked down for BRCA1 or CAMP using siRNA. N=3 biologically independent experiments. Error bars indicate standard errors, and p values were calculated using two-tailed Student t-test, ***P<0.0001. **b**, Graph showing the percentage of GFP-positive cells after EJ5-GFP analysis. U2OS cells were infected with I-SceI adenovirus and knocked down for 53BP1 or CAMP using siRNA. N=3 biologically independent experiments. Error bars indicate standard errors, and p values were calculated using two-tailed Student t-test, ***P<0.0001, **P<0.001,*P<0.05. **c**, Quantification of resected ssDNA measured by SMART assay in U2OS cells treated by siControl or siRNAs targeting CAMP for 48hrs. Approximately 50 fibers were counted per experiment. Error bars indicate standard errors, and p values were calculated using Student t-test, ***P<0.0001. **d**, (left) Representative images of RAD51 foci formation in wild-type and two CAMP knockout U2OS cell lines 6 hours after 5Gy IR treatment. (right) Quantification of >10 RAD51 foci. n=3 biologically independent experiments. ***P < 0.001. Statistical analysis was performed using two-tailed student's t-tests. **e**, 5-day cytotoxicity analysis of wild type and two CAMP knockout RPE1(p53-/-) cell lines treated with various doses of olaparib; n=3 independent experiments. Wild type versus CAMP-KO#1, ***P<0.0001; Wild type versus CAMP-KO#2, ***P<0.0001; statistical analysis was performed using two-way ANOVA. **f**, 5-day cytotoxicity analysis of wild type and two CAMP knockout U2OS cell lines treated with various doses of olaparib; n=3 independent experiments. Wild type versus CAMP-KO#1, ***P<0.0001; Wild type versus CAMP-KO#2, ***P<0.0001; statistical analysis was performed using two-way ANOVA.

Figure 2. DNA Damage Activates REV7 seatbelt closure and partner protein binding

a, 293T cells were transfected with FLAG-REV7-WT or FLAG-REV7-T103A, and following treatment with/without UV (20J/m^2) for 1 hour. The FLAG-immunoprecipitations were detected by western blot using anti-Flag and anti-p-[S/T]Q antibodies. **b**, 293T cells were transfected with FLAG-REV7-WT or FLAG-REV7-T103A, and following treatment with/without UV (20J/m^2) as indicated. Western blot showing chromatin fraction of FLAG-REV7-WT and FLAG-REV7-T103A. Histone H3 is used as control for chromatin isolation. **c**, Western blot showing chromatin fraction of REV7 in U2OS treated with DMSO or ATM inhibitor, following IR treatment as indicated. **d**, Schematic of our proposed model showing that the conformational state is regulated by TRIP1-p31 complex and ATM. ATM phosphorylates REV7 at T103 site and promotes the closed form of REV7. The closed REV7 interacts with CAMP, SHLD3 and REV3. **e**, Western blot showing GFP-immunoprecipitation of GFP-CAMP in wild-type (WT), *TRIP13*$^{-/-}$ and p31$^{-/-}$ U2OS cells, and the co-immunoprecipitation of endogenous REV7. **f**, Western blot showing GFP-immunoprecipitation of GFP-CAMP in U2OS-vector control (VC) and TRIP13 overexpressed U2OS cells, and the co-immunoprecipitation of endogenous TRIP13 and REV7. **g**, 293T cells were co-transfected with GFP-SHLD3 and Flag-REV7 or Flag-REV7-T103A. Western blot showing GFP-immunoprecipitation of GFP-SHLD3, and the co-immunoprecipitation of Flag-REV7 and Flag-REV7-T103A. **h**, Western blot showing Flag-immunoprecipitation of Flag-REV7 wild type and Flag-REV7-T103A mutant, and the co-immunoprecipitation of endogenous CAMP. **i**, 293T cells were co-transfected with GFP-tagged fragment of REV3 containing the REV7-binding domain (R3BD) and Flag-REV7 or Flag-

REV7-T103A. Western blot showing Flag-immunoprecipitation of Flag-REV7 and Flag-REV7-T103A, and the co-immunoprecipitation of GFP-R3BD.

Figure 3. CAMP competes with SHLD3 and REV3 for binding to REV7

a, Western blot showing GFP-immunoprecipitation of GFP-SHLD3 in 293T cells, treated with or without siCAMP, and the co-immunoprecipitation of endogenous CAMP and REV7. **b**, Western blot showing GFP-immunoprecipitation of GFP-tagged fragment of REV3 containing the REV7 binding domain (R3BD) in U2OS wild type and U2OS$^{CAMP-/-}$ cells, and the co-immunoprecipitation of endogenous CAMP and REV7. **c**, A 14 days clonogenic assay of U2OS wild type and two CAMP-KO U2OS cell lines, treated with various doses of MMC; n=3 independent experiments. *P<0.05. Statistical analysis was performed using two-way ANOVA. **d**, A 14 days clonogenic assay of RPE1$^{p53-/-}$ and two RPE1$^{p53-/-CAMP-/-}$ cell lines, treated with various doses of MMC; n=3 independent experiments. *P<0.05. Statistical analysis was performed using two-way ANOVA. **e**, (left) Schematic of our proposed model of CAMP function in HR, c-NHEJ and TLS regulation. (right) The table showing summary of Olaparib and MMC sensitivity of indicated cells.

Figure 4. The REV7 binding region of CAMP is required for the HR function but not for correction of chromosome misalignment

a, (Top) Schematic of CAMP protein showing its various domains and REV7 binding region. (Bottom) Schematic of CAMP-Full Length (FL) and two mutants (2A and ΔFPE). SBM, REV7 seatbelt binding motif. **b**, Structure of the REV7-CAMP complex. REV7 is shown in cyan and blue (seatbelt domain), and the CAMP fragment (residues 331-343) is shown in red. **c**, Western

blot showing GFP-immunoprecipitation of GFP-Empty Vector, GFP-CAMP wild-type, GFP-CAMP-2A mutant or GFP-CAMP-ΔFPE, and the co-immunoprecipitation of endogenous REV7 in 293T cells. **d**, A 14 days clonogenic assay of indicated cell lines treated with various doses of Olaparib; n=3 independent experiments, **P<0.001. Statistical analysis was performed using two-way ANOVA. **e**, Summary of chromosome misalignment in indicated cell lines. **f**, Quantitative analysis of indicated cells in G2/M.

Figure 5. CAMP is epistatic to REV7 in the Regulation of Homologous Recombination

Quantification of RAD51 (**a**) and p-RPA32(S33) (**b**) foci formation in wild-type and *REV7*$^{-/-}$ U2OS cells treated with siRNA negative control (siNC) and siCAMP, and 6 hours after 5Gy IR treatment.. More than 10 RAD51 foci were counted. n=3 biologically independent experiments, ***P < 0.0001. Statistical analysis was performed using two-tailed student's t-tests. **c**, A 14-days clonogenic survival of wild-type and REV7$^{-/-}$ U2OS cells treated with various doses of Olaparib after siControl or siCAMP treatment. n=3 independent experiments, **P < 0.001, ***P < 0.0001. Statistical analysis was performed using two-way ANOVA. **d**, A 14-days clonogenic survival of RPE1$^{p53-/-}$, RPE1$^{p53-/-BRCA1-/-}$ and niraparib/olaparib-resistant RPE1$^{p53-/-BRCA1-/-}$ cell clones treated with various doses of Olaparib after siControl or siCAMP treatment. n=3 independent experiments. Statistical analysis was performed using two-way ANOVA. **e**, Kaplan–Meier curves depicting overall survival of ovarian cancer patients with CAMP expression and REV7 expression. **f**, CAMP expression positively correlates with Cyclin E expression. **g**, Breast cancer cells with high expression of CCNE1 are more dependent on CAMP for survival.

EXTENDED FIGURE LEGENDS

Extended Data Figure 1, related to Fig. 1.

a, Western blot showing knocking down efficiency of siRNA targeting CAMP. U2OS cells were treated with siRNA negative control or siCAMP for 48hrs. **b**, A 14 days clonogenic assay of RPE1 cells treated with siRNA control and siCAMP, and treated with various doses of olaparib; n=3 independent experiments, ***P<0.0001. Statistical analysis was performed using two-way ANOVA. **c**, Western blot showing the lack of CAMP expression in two CAMP knockout RPE1 cell lines. **d**, Western blot showing the lack of CAMP expression in two CAMP knockout U2OS cell lines. **e**, Western blot showing FLAG-immunoprecipitation of FLAG-CAMP, and the co-immunoprecipitation of endogenous REV7 in HEK293T cells. **f**, Representative images of CAMP and REV7 foci 1h after UV treatment in U2OS cells. co-localizations of CAMP and REV7 are shown as indicated. DAPI was used to stain the nuclei. **g**, Quantification of CAMP-REV7 foci co-localization shown in (A). n=3 independent experiments. Error bars indicate standard errors, and p values were calculated using two-tailed Student t-test, ***P<0.0001. **h**, Chromatin fraction of CAMP and REV7 in U2OS wild-type and CAMP-KO cells with or without UV (20J/m^2) treatment as indicate. Histone H3 is used as control for chromatin isolation. **i**, Quantification of Chromatin-bound REV7 in (h).

Extended Data Figure 2, related to Fig. 2.

a, Primary sequence alignment of REV7 and MAD2 from various organisms. **b**, Structure of the closed form of REV7 and closed form of MAD2. C-REV7 is shown in purple and orange (seatbelt domain). C-MAD2 is shown in green and orange (seatbelt domain). **c**, 293T cells were transfected with FLAG-REV7, and following treatment with UV (20J/m^2) for 1 hour or IR (5Gy)

for 2 hours. The FLAG-immunoprecipitations were detected by western blot using anti-Flag and anti-p-[S/T]Q antibodies. **d**, Western blot showing phosphor-KAP1 in U2OS cells treated with/without ATM inhibitor, following IR treatment as indicated. **e**, Quantitative analysis of REV7 foci formation in wild type, TRIP13-/-, REV7-/-, TRIP13-overexpressed and ATMi treated U2OS cells after IR (5Gy) treatment. **f**, Representative images of REV7 foci formation in 293T cells expressing Flag-tagged wild type REV7 and REV7-T103A mutant. DAPI was used to stain the nuclei. **g**, REV7-KO U2OS cells were transfected with GFP-Empty Vector, Flag-REV7 wild-type or Flag-T103A mutant, following with/without IR treatment as indicated. **h**, Quantification of >10 RAD51 foci. Error bars indicate standard errors, and p values were calculated using two-tailed Student t-test, ***P<0.0001. **i**, U2OS-REV7$^{-/-}$ cells were transfected with Empty Vector, Flag-REV7 wild-type or REV7-T103A mutant, then detected by western blot using anti-REV7. Actin acts as loading control. **j**. A 14 days clonogenic assay of same cell lines in (i) treated with various doses of olaparib; n=3 independent experiments, *P<0.05. Statistical analysis was performed using two-way ANOVA.

Extended Data Figure 3, related to Fig. 3.

a, Representative images of metaphase spreads from RPE1$^{p53-/-}$ and RPE1$^{p53-/-CAMP-/-}$ cells. Arrows show the chromosome dicentrics. **b**, Table summarizing chromosome radial formation and chromosome dicentrics in RPE1$^{p53-/-}$, RPE1$^{p53-/-REV7-/-}$, RPE1$^{p53-/-CAMP-/-}$#1, and RPE1$^{p53-/-CAMP-/-}$#2 cells.

Extended Data Figure 4, related to Fig. 4.

a, CAMP knockout induced chromosome misalignment. RPE1$^{p53-/-}$ and RPE1$^{p53-/-CAMP-/-}$ cells were stained with anti-tubulin and anti-CENP-A. DNA was stained with DAPI. **b**, Quantitative analysis of chromosome misalignment in CAMP depleted RPE1 cells. **c**, U2OS cells were transfected with GFP-Empty Vector, CAMP wild-type and CAMP-2A mutant. Western blot showing the expression of CAMP. GAPDH acts as loading control. A 14 days clonogenic assay of same cell lines in (c) treated with various doses of Olaparib (**d**) or MMC (**e**); n=3 independent experiments, *P<0.05. Statistical analysis was performed using two-way ANOVA. **f**, U2OS$^{CAMP-/-}$ cells were transfected with GFP-Empty Vector, GFP-CAMP wild-type or GFP-CAMP-2A mutant. Western blot showing the expression of CAMP. GAPDH acts as loading control. **g**, A 14 days clonogenic assay of same cell lines in (f) treated with various doses of Olaparib; n=3 independent experiments, *P<0.05. Statistical analysis was performed using two-way ANOVA.

Extended Data Figure 5, related to Fig. 5.

a, Representative images of RAD51 foci formation in wild-type and *REV7*$^{-/-}$ U2OS cells treated with siRNA negative control (siNC) and siCAMP, and 6 hours after 5Gy IR treatment. **b**, Representative images of p-RPA32(S33) foci formation in wild-type and *REV7*$^{-/-}$ U2OS cells treated with siRNA negative control (siNC) and siCAMP, and 6 hours after 5 Gy IR treatment. **c**, A 14 days clonogenic assay of HCC1937 cells (SHLD2 deficient) treated with siControl or siCAMP with various doses of olaparib. Western blot showing the expression of CAMP. Actin acts as loading control. **d**, Schematic of PARPi-resistant RPE1$^{p53-/-BRCA1-/-}$ cells generation. RPE1$^{p53-/-BRCA1-/-}$ cells (B40) were treated with increasing concentrations of the PARPis niraparib/olaparib over 3 months, and then isolated by single-cell clones from the niraparib- and olaparib-resistant pools. **e**, Western blot showing the expression of CAMP in acquired PRAPi

resistant single clones. **f**, CAMP is highly expressed in BRCA2 mutated tumors. Kaplan–Meier curves depicting overall survival of patients from TCGA with CAMP expression and wildtype BRCA1 and BRCA2 (**g**), and mutated BRCA1 or BRCA2 (**h**). This analysis combines tumors from these TCGA studies: BLCA (blader), BRCA (breast), LUAD (lung), LUSC (lung squamous), and SKCM (skin).

Materials and Methods

Cell culture and transfections

Human U2OS, RPE1-hTERT, HCC1937 and HEK293T cells were cultured in DMEM/F12 + Glutamax (Invitrogen) supplemented with 10% FBS (Sigma) and 1% penicillin-streptomycin (Invitrogen). DNA transfections and siRNA knockdowns were carried out using Lipofectamine LTX (Invitrogen) and RNAiMax (Invitrogen) respectively according to the manufacturer's protocols. The individual siRNAs used are: AllStar negative siControl (1027281); siCAMP #4 (SI00973084); siCAMP #8 (SI04282159); siBRCA1 (SI00930510); si53BP1 (SI01456539) were purchased from Qiagen.

Antibodies and chemicals

Antibodies used in this study were: Abnova H00283489-B01P (C13orf8/CAMP, IB, IF), Abcam ab180579 (Mad2L2/REV7, IB), Abcam ab128171 (TRIP13, IB), Cell Signaling 3873 (alpha-Tubulin, IF), Cell Signaling 2187 (Phospho-CENP-A, IF), Cell Signaling 3638 (H3, IB), Cell Signaling 2956 (GFP, IB), Cell Signaling 3700 (Actin, IB), Abcam ab70369 (phospho-Kap1-S824, IB), Cell Signaling 6966 (Phospho-[S/T]Q, IB), Fisher Scientific NB100544 (RPA2-P-Ser33, IF), Santa Cruz sc-8349 (RAD51, IF), Millipore-Sigma F3165 (GAPDH, IB) and Millipore-Sigma F3165 (Flag, IB, IF). Mitomycin C (MMC) was purchased from Sigma and Olaparib was purchased from Selleckchem.

Generation of knockout cell lines with CRISPR-Cas9

CAMP guide RNA sequences were cloned into the pSpCas9 BB-2A-GFP (PX458) vector (GenScript). U2OS and RPE1$^{p53-/-}$ cells were transfected with Cas9-gRNA plasmids. After 48 hours GFP positive cells were selected using a BD FACSAria II cell sorter. Single cells from GFP positive pool were cultured for three to four weeks and colonies were screened for

knockouts by western blotting using the anti-p31^{comet} antibody (Millipore-Sigma). The guide RNA sequences targeting CAMP in this study were: #1 TCGTAAACCATCAGCACGTT and #2 CCAGAGATCCGTAGTCCAGC.

GFP-based DNA Repair Assays

For DR- and EJ5-GFP reporter assays, U2OS cells carrying the respective GFP expression cassette were transfected with the indicated siRNAs. 24 hours after transfection, cells were infected with or without I-SceI lentivirus. After 48 hours, cells were harvested and detected by flow cytometry. The data was analyzed using the FlowJo software.

Cellular fractionation and immunoblot analysis

Cells were lysed with NP40 buffer (1% NP40, 300 mM NaCl, 0.1 mM EDTA, 50 mM Tris (pH 7.5)) supplemented with phosphatase and protease inhibitor cocktail (Roche). Cell lysates were resolved by NuPAGE 4-12% Bis-Tris gels (Invitrogen), and transferred onto nitrocellulose membranes. Membranes were blocked with 5% BSA in TBST and were sequentially incubated with primary and secondary antibodies and detected using chemiluminescence or fluorescence (LI-COR Biosciences). For chromatin extraction, chromatin-bound extracts were got using subcellular protein fractionation kit (Thermo).

Immunoprecipitation

After transfection for 48h, 293T or U2OS cells were then harvested and lysed in NETN lysis buffer with proteinase & phosphatase inhibitor cocktail (Thermo, 1:100) for 30 minutes on ice. They were then incubated with antibody-bead conjugate (Anti-FLAG® M2 Magnetic Beads, Millipore & Sigma or GFP-Trap_A, Chromotek) overnight at 4 °C. Beads were washed four times with NETN buffer and immunoprecipitates were eluted by boiling.

Drug sensitivity assays

Cells were transfected with plasmid or siRNA 24h before being plated for colony formation or CellTiter-Glo assays. To assay clonogenic survival, cells were seeded at 500-1000 cells/well in 6-well plates in triplicates. Drugs at the shown doses were added after 12 hours and cells were permitted to grow for 14 days. Colony formation was scored by fixing and staining with 0.5% (w/v) crystal violet in 20% methanol. For short term CellTiter-Glo survival assays, cells were plated in 96-well plates at 800-1000 cells/well, and treated with drugs at the indicated concentrations after 12 hours. Three days later, cellular viability was measured using CellTiter-Glo (Promega). Survival at each drug concentration was calculated as a percentage normalized to the corresponding untreated control, for both assays.

Immunofluorescence assays

Cells were plated on glass coverslips in 12-well plates. They were then either left untreated or treated at 20J/m^2 UV or 5Gy IR. After 1 or 6 hours, they were harvested by pre-extraction with 0.5% Triton X-100 for 5 min, followed 4% paraformaldehyde fixation for 10 min at 4 °C. After three PBS washes, blocking was performed with 3% BSA in PBS for 1 hour at room temperature, followed by sequential primary and secondary antibody incubations overnight at 4 °C and 1 hour at room temperature respectively. The coverslips were mounted with DAPI (Vector Laboratories) and captured using a Zeiss AX10 fluorescence microscope and Zen software, and foci were scored. At least 100 cells were counted for each sample.

Chromosomal aberration analysis

RPE1$^{p53-/-}$ and RPE1$^{p53-/-CAMP-/-}$ cells were incubated with or without 20 ng/ml MMC for 48 hours. Cells were treated with 100 ng/ml of colcemid for 2 hours, followed by a hypotonic solution (0.075 M KCl) for 20 min and fixed with 3:1 methanol/acetic acid. After staining with Wright's

stain, 50 metaphase spreads were counted for aberrations. The relative number of chromosomal dicentrics and radials was calculated relative to control cells as indicated.

TCGA data acquisition and analysis

The survival analyses of the Cancer Genome Atlas (TCGA) patients were performed using the clinical and RNASeq expression and genomic alteration data of TCGA Pan-Cancer study for 32 cancer types downloaded from the cBioPortal for Cancer Genomics (https://www.cbioportal.org; retrieved March 2020). For the survival analysis with mRNA expression of CAMP (CHAMP1) and REV7 (MAD2L2), for each cancer type, samples were grouped into the low- and high-mRNA expressing groups for CAMP and REV7 based on the expression z-scores of either zero, or less than -0.5 and greater than 0.5. These expression z-scores were computed relative to the diploid samples. Survival analysis was then performed in R for each cancer type to determine whether there was a difference in the overall survival between the two groups, separately for CAMP and REV7, and for REV7 in each of the two CAMP groups. Kaplan-Meier curves were created, and the log-rank test was used to test for a difference in overall survival using the survival package in R. The p values were calculated from the chi-square distribution. The survminer R package was used to estimate median survivals, and to plot the Kaplan-Meier curves. Additionally, Cox proportional hazards regression was performed to estimate the hazard ratio between the low- and the high-mRNA groups for each cancer type.

The survival analyses of TCGA patients with CAMP mRNA expression and mutation status of BRCA1 and BRCA2 were performed as follows. A tumor was considered mutated for a gene if it had variants with classifications that were damaging or other non-conserving. The analyses were first performed for each cancer type and independently with mutation status of BRCA1 and BRCA2. Then the cancer types that showed a trend from the results with either gene were

selected for the combined analysis. The combined survival analysis with CAMP expression and mutation status of BRCA1 and BRCA2 was performed with tumors being considered mutated if they had a mutated status for either BRCA1 or BRCA2. Also, the Cox proportional hazards regression was performed with accounting for the differences between cancer types and between tumor stages.

Cancer cell lines' data acquisition and analysis

The association analyses between cyclin E (CCNE1) expression and CAMP (CHAMP1) dependency and CAMP expression in cancer cell lines were performed using the expression data from the Cancer Cell Line Encyclopedia (CCLE) project [30] and the dependency data from the Broad Institute Cancer Dependency Map (DepMap; CRISPR DepMap Public 19Q4 dataset) [31]. Both datasets were downloaded from the DepMap Portal (https://depmap.org/portal/). The RNASeq expression counts were normalized by the TMM (weighted trimmed mean of M-values) method using the edgeR package [32] and transformed into log2-counts per million (log2-CPM) values. For each cancer lineage, the low- and high-cyclin E mRNA expressing groups were determined using the median log2-CPM. The significance of the difference in the CAMP dependency between the low- and high-cyclin E mRNA groups were assessed by the Wilcoxon rank sum test using the ggpubr R package. The correlation between CAMP mRNA expression and cyclin E mRNA expression were performed by the simple linear regression on the log2-CPM values using the ggpmisc R package. The plots were generated using the ggplot2 package in R.

REFERENCES

1 Clairmont, C. S. & D'Andrea, A. D. REV7 directs DNA repair pathway choice. *Trends Cell Biol*, doi:10.1016/j.tcb.2021.05.009 (2021).

2 de Krijger, I., Boersma, V. & Jacobs, J. J. L. REV7: Jack of many trades. *Trends Cell Biol*, doi:10.1016/j.tcb.2021.04.002 (2021).

3 Hara, K. *et al.* Crystal structure of human REV7 in complex with a human REV3 fragment and structural implication of the interaction between DNA polymerase zeta and REV1. *J Biol Chem* **285**, 12299-12307, doi:10.1074/jbc.M109.092403 (2010).

4 Dev, H. *et al.* Shieldin complex promotes DNA end-joining and counters homologous recombination in BRCA1-null cells. *Nat Cell Biol* **20**, 954-965, doi:10.1038/s41556-018-0140-1 (2018).

5 Ghezraoui, H. *et al.* 53BP1 cooperation with the REV7-shieldin complex underpins DNA structure-specific NHEJ. *Nature* **560**, 122-127, doi:10.1038/s41586-018-0362-1 (2018).

6 Gupta, R. *et al.* DNA Repair Network Analysis Reveals Shieldin as a Key Regulator of NHEJ and PARP Inhibitor Sensitivity. *Cell* **173**, 972-988 e923, doi:10.1016/j.cell.2018.03.050 (2018).

7 Mirman, Z. *et al.* 53BP1-RIF1-shieldin counteracts DSB resection through CST- and Polalpha-dependent fill-in. *Nature* **560**, 112-116, doi:10.1038/s41586-018-0324-7 (2018).

8 Noordermeer, S. M. *et al.* The shieldin complex mediates 53BP1-dependent DNA repair. *Nature* **560**, 117-121, doi:10.1038/s41586-018-0340-7 (2018).

9 Hara, K. *et al.* Dynamic feature of mitotic arrest deficient 2-like protein 2 (MAD2L2) and structural basis for its interaction with chromosome alignment-maintaining phosphoprotein (CAMP). *J Biol Chem* **292**, 17658-17667, doi:10.1074/jbc.M117.804237 (2017).

10 Itoh, G. *et al.* CAMP (C13orf8, ZNF828) is a novel regulator of kinetochore-microtubule attachment. *EMBO J* **30**, 130-144, doi:10.1038/emboj.2010.276 (2011).

11 Clairmont, C. S. *et al.* TRIP13 regulates DNA repair pathway choice through REV7 conformational change. *Nat Cell Biol* **22**, 87-96, doi:10.1038/s41556-019-0442-y (2020).

12 Sarangi, P., Clairmont, C. S., Galli, L. D., Moreau, L. A. & D'Andrea, A. D. p31(comet) promotes homologous recombination by inactivating REV7 through the TRIP13 ATPase. *Proc Natl Acad Sci U S A* **117**, 26795-26803, doi:10.1073/pnas.2008830117 (2020).

13 Isidor, B. *et al.* De Novo Truncating Mutations in the Kinetochore-Microtubules Attachment Gene CHAMP1 Cause Syndromic Intellectual Disability. *Hum Mutat* **37**, 354-358, doi:10.1002/humu.22952 (2016).

14 Pierce, A. J., Johnson, R. D., Thompson, L. H. & Jasin, M. XRCC3 promotes homology-directed repair of DNA damage in mammalian cells. *Genes Dev* **13**, 2633-2638, doi:10.1101/gad.13.20.2633 (1999).

15 Stark, J. M., Pierce, A. J., Oh, J., Pastink, A. & Jasin, M. Genetic steps of mammalian homologous repair with distinct mutagenic consequences. *Mol Cell Biol* **24**, 9305-9316, doi:10.1128/MCB.24.21.9305-9316.2004 (2004).

16 Symington, L. S. End resection at double-strand breaks: mechanism and regulation. *Cold Spring Harb Perspect Biol* **6**, doi:10.1101/cshperspect.a016436 (2014).

17 Huertas, P. & Cruz-Garcia, A. Single Molecule Analysis of Resection Tracks. *Methods Mol Biol* **1672**, 147-154, doi:10.1007/978-1-4939-7306-4_12 (2018).

18 Bryant, H. E. *et al.* Specific killing of BRCA2-deficient tumours with inhibitors of poly(ADP-ribose) polymerase. *Nature* **434**, 913-917, doi:10.1038/nature03443 (2005).

19 Farmer, H. *et al.* Targeting the DNA repair defect in BRCA mutant cells as a therapeutic strategy. *Nature* **434**, 917-921, doi:10.1038/nature03445 (2005).
20 Boersma, V. *et al.* MAD2L2 controls DNA repair at telomeres and DNA breaks by inhibiting 5' end resection. *Nature* **521**, 537-540, doi:10.1038/nature14216 (2015).
21 Xu, G. *et al.* REV7 counteracts DNA double-strand break resection and affects PARP inhibition. *Nature* **521**, 541-544, doi:10.1038/nature14328 (2015).
22 Matsuoka, S. *et al.* ATM and ATR substrate analysis reveals extensive protein networks responsive to DNA damage. *Science* **316**, 1160-1166, doi:10.1126/science.1140321 (2007).
23 Farkkila, A. *et al.* Heterogeneity and Clonal Evolution of Acquired PARP Inhibitor Resistance in TP53- and BRCA1-Deficient Cells. *Cancer Res* **81**, 2774-2787, doi:10.1158/0008-5472.CAN-20-2912 (2021).
24 Baude, A. *et al.* Hepatoma-derived growth factor-related protein 2 promotes DNA repair by homologous recombination. *Nucleic Acids Res* **44**, 2214-2226, doi:10.1093/nar/gkv1526 (2016).
25 Daugaard, M. *et al.* LEDGF (p75) promotes DNA-end resection and homologous recombination. *Nat Struct Mol Biol* **19**, 803-810, doi:10.1038/nsmb.2314 (2012).
26 Nozawa, R. S. *et al.* Human POGZ modulates dissociation of HP1alpha from mitotic chromosome arms through Aurora B activation. *Nat Cell Biol* **12**, 719-727, doi:10.1038/ncb2075 (2010).
27 Vermeulen, M. *et al.* Quantitative interaction proteomics and genome-wide profiling of epigenetic histone marks and their readers. *Cell* **142**, 967-980, doi:10.1016/j.cell.2010.08.020 (2010).
28 Soria, G. & Almouzni, G. Differential contribution of HP1 proteins to DNA end resection and homology-directed repair. *Cell Cycle* **12**, 422-429, doi:10.4161/cc.23215 (2013).
29 Olivieri, M. *et al.* A Genetic Map of the Response to DNA Damage in Human Cells. *Cell* **182**, 481-496 e421, doi:10.1016/j.cell.2020.05.040 (2020).
30 Ghandi, M. *et al.* Next-generation characterization of the Cancer Cell Line Encyclopedia. *Nature* **569**, 503-508, doi:10.1038/s41586-019-1186-3 (2019).
31 Meyers, R. M. *et al.* Computational correction of copy number effect improves specificity of CRISPR-Cas9 essentiality screens in cancer cells. *Nat Genet* **49**, 1779-1784, doi:10.1038/ng.3984 (2017).
32 Robinson, M. D., McCarthy, D. J. & Smyth, G. K. edgeR: a Bioconductor package for differential expression analysis of digital gene expression data. *Bioinformatics* **26**, 139-140, doi:10.1093/bioinformatics/btp616 (2010).

Figures

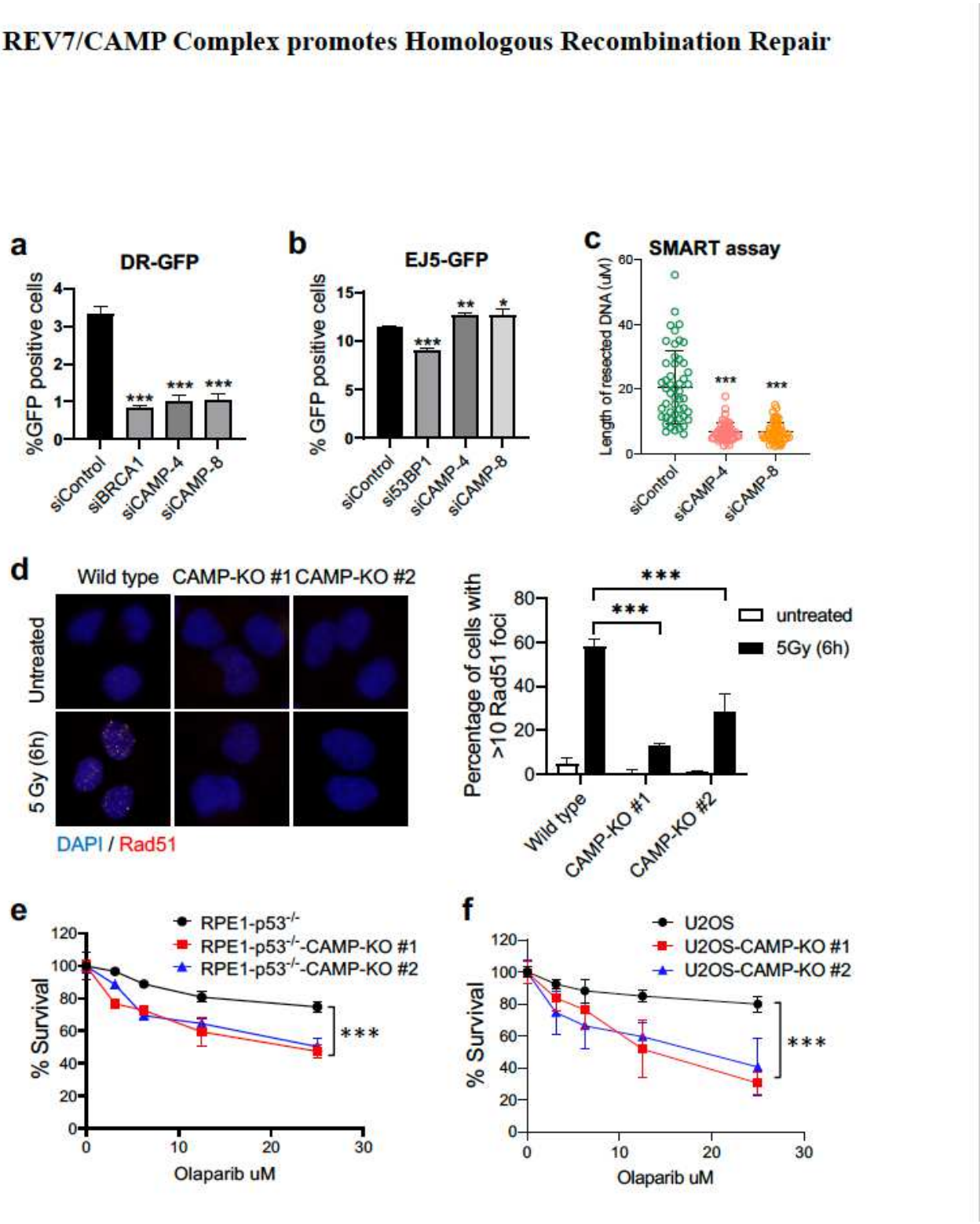

Figure 1

CAMP promotes homologous recombination a, Graph showing the percentage of GFP-positive cells after DR-GFP analysis. U2OS cells were infected with I-SceI adenovirus and knocked down for BRCA1 or CAMP using siRNA. N=3 biologically independent experiments. Error bars indicate standard errors, and p values

were calculated using two-tailed Student t-test, ***P<0.0001. b, Graph showing the percentage of GFP-positive cells after EJ5-GFP analysis. U2OS cells were infected with I-SceI adenovirus and knocked down for 53BP1 or CAMP using siRNA. N=3 biologically independent experiments. Error bars indicate standard errors, and p values were calculated using two-tailed Student t-test, ***P<0.0001, **P<0.001,*P<0.05. c, Quantification of resected ssDNA measured by SMART assay in U2OS cells treated by siControl or siRNAs targeting CAMP for 48hrs. Approximately 50 fibers were counted per experiment. Error bars indicate standard errors, and p values were calculated using Student t-test, ***P<0.0001. d, (left) Representative images of RAD51 foci formation in wild-type and two CAMP knockout U2OS cell lines 6 hours after 5Gy IR treatment. (right) Quantification of >10 RAD51 foci. n=3 biologically independent experiments. ***P < 0.001. Statistical analysis was performed using two-tailed student's t-tests. e, 5-day cytotoxicity analysis of wild type and two CAMP knockout RPE1(p53-/-) cell lines treated with various doses of olaparib; n=3 independent experiments. Wild type versus CAMP-KO#1, ***P<0.0001; Wild type versus CAMP-KO#2, ***P<0.0001; statistical analysis was performed using two-way ANOVA. f, 5-day cytotoxicity analysis of wild type and two CAMP knockout U2OS cell lines treated with various doses of olaparib; n=3 independent experiments. Wild type versus CAMP KO#1, ***P<0.0001; Wild type versus CAMP-KO#2, ***P<0.0001; statistical analysis was performed using two-way ANOVA.

Fig 2. DNA Damage Activates REV7 seatbelt closure and partner protein binding

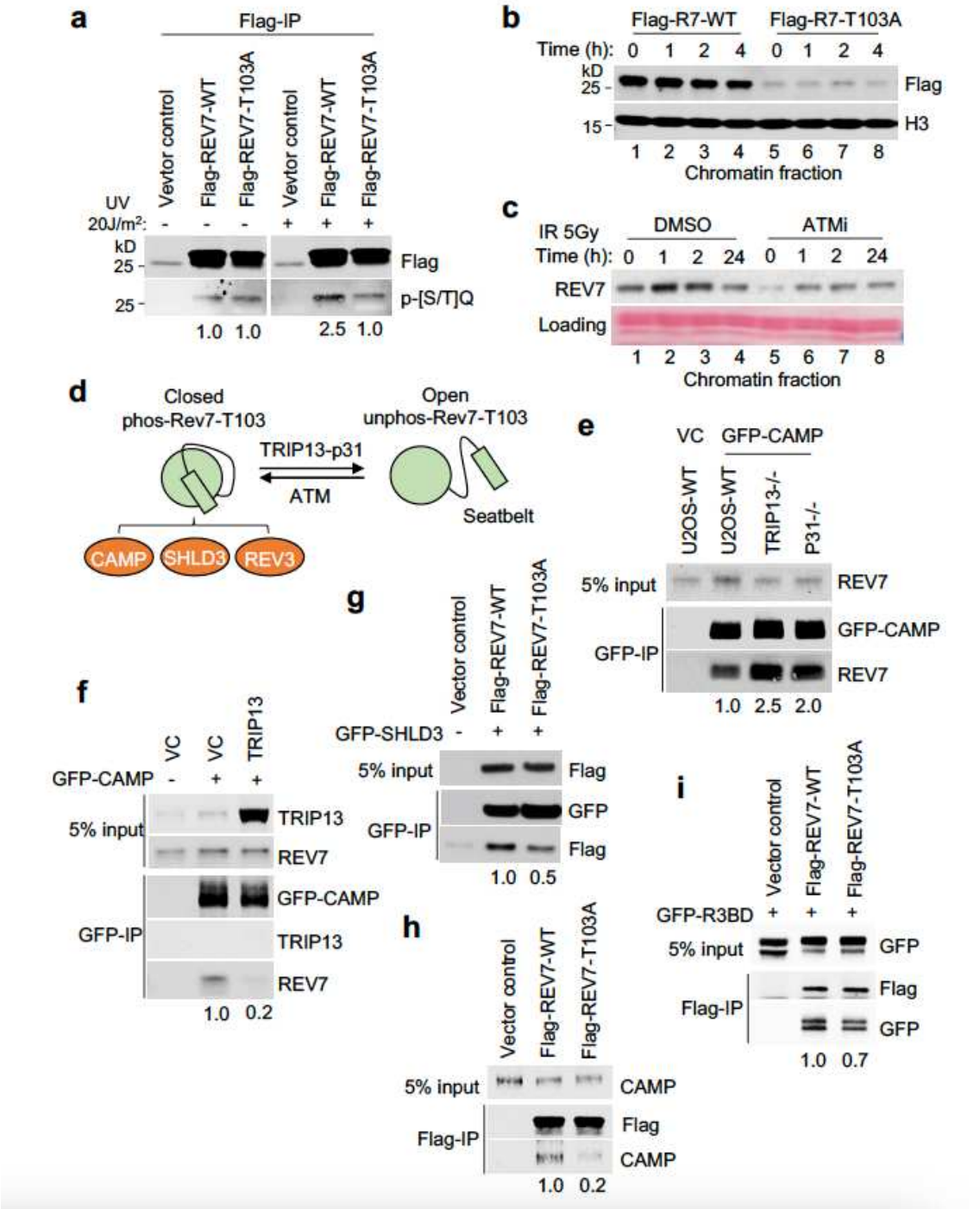

Figure 2

DNA Damage Activates REV7 seatbelt closure and partner protein binding a, 293T cells were transfected with FLAG-REV7-WT or FLAG-REV7-T103A, and following treatment with/without UV (20J/m2) for 1 hour. The FLAG-immunoprecipitations were detected by western blot using anti-Flag and anti-p-[S/T]Q antibodies. b, 293T cells were transfected with FLAG-REV7-WT or FLAG-REV7-T103A, and following treatment with/without UV (20J/m2) as indicated. Western blot showing chromatin fraction of FLAG-

REV7-WT and FLAG-REV7- T103A. Histone H3 is used as control for chromatin isolation. c, Western blot showing chromatin fraction of REV7 in U2OS treated with DMSO or ATM inhibitor, following IR treatment as indicated. d, Schematic of our proposed model showing that the conformational state is regulated by TRIP1-p31 complex and ATM. ATM phosphorylates REV7 at T103 site and promotes the closed form of REV7. The closed REV7 interacts with CAMP, SHLD3 and REV3. e, Western blot showing GFP-immunoprecipitation of GFP-CAMP in wild-type (WT), TRIP13-/- and p31-/- U2OS cells, and the co-immunoprecipitation of endogenous REV7. f, Western blot showing GFP-immunoprecipitation of GFP-CAMP in U2OS-vector control (VC) and TRIP13 overexpressed U2OS cells, and the co-immunoprecipitation of endogenous TRIP13 and REV7. g, 293T cells were co-transfected with GFP-SHLD3 and Flag-REV7 or Flag-REV7- T103A. Western blot showing GFP-immunoprecipitation of GFP-SHLD3, and the co-immunoprecipitation of Flag-REV7 and Flag-REV7-T103A. h, Western blot showing Flag immunoprecipitation of Flag-REV7 wild type and Flag-REV7-T103A mutant, and the co-immunoprecipitation of endogenous CAMP. i, 293T cells were co-transfected with GFP-tagged fragment of REV3 containing the REV7-binding domain (R3BD) and Flag-REV7 or Flag

Fig 3. CAMP competes with SHLD3 and REV3 for binding to REV7

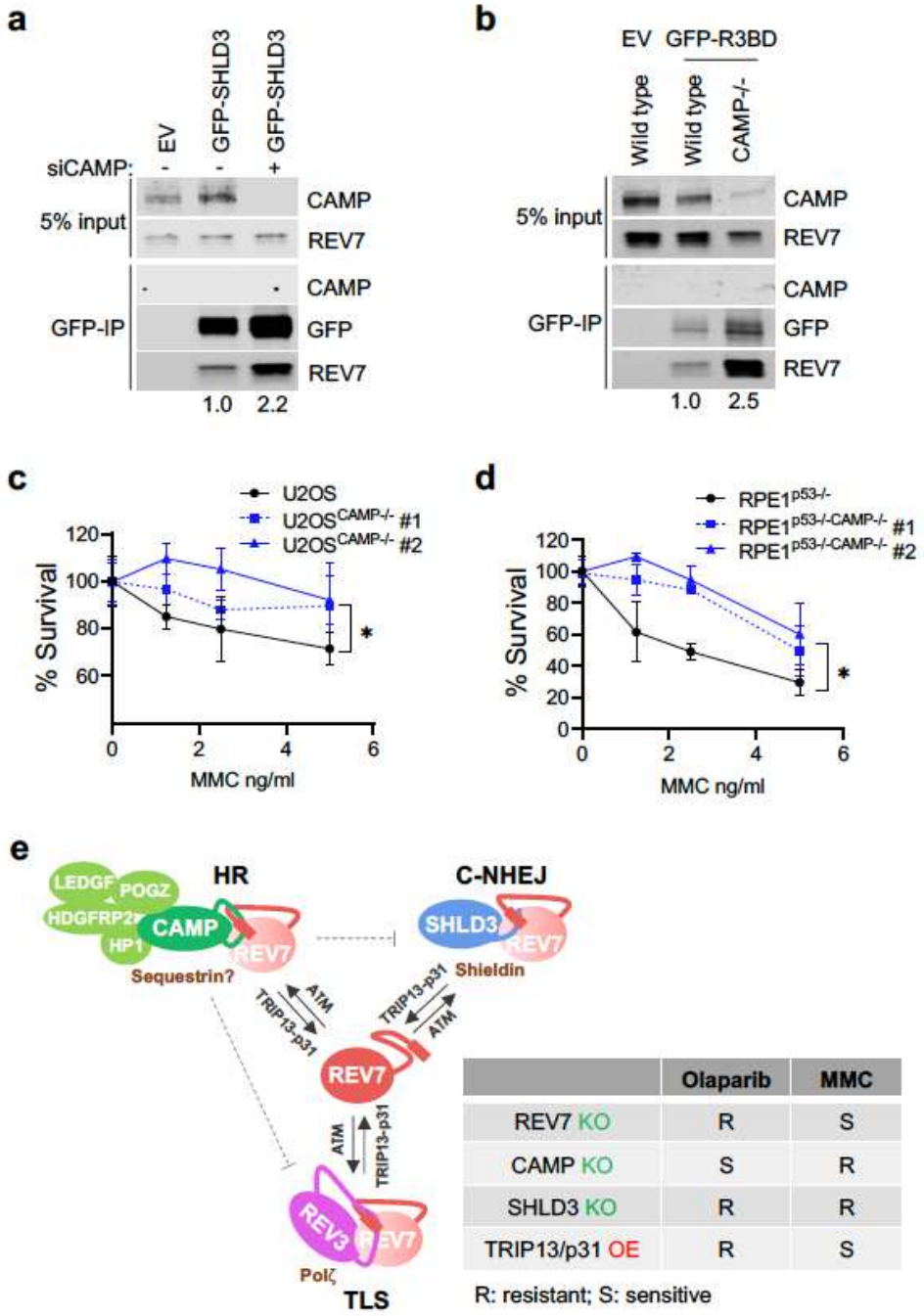

	Olaparib	MMC
REV7 KO	R	S
CAMP KO	S	R
SHLD3 KO	R	R
TRIP13/p31 OE	R	S

R: resistant; S: sensitive

Figure 3

CAMP competes with SHLD3 and REV3 for binding to REV7 a, Western blot showing GFP-immunoprecipitation of GFP-SHLD3 in 293T cells, treated with or without siCAMP, and the co-immunoprecipitation of endogenous CAMP and REV7. b, Western blot showing GFP-immunoprecipitation of GFP-tagged fragment of REV3 containing the REV7 binding domain (R3BD) in U2OS wild type and U2OSCAMP-/- cells, and the co-immunoprecipitation of endogenous CAMP and REV7. c, A 14 days

clonogenic assay of U2OS wild type and two CAMP-KO U2OS cell lines, treated with various doses of MMC; n=3 independent experiments. *P<0.05. Statistical analysis was performed using two-way ANOVA. d, A 14 days clonogenic assay of RPE1p53-/- and two RPE1p53-/-CAMP-/- cell lines, treated with various doses of MMC; n=3 independent experiments. *P<0.05. Statistical analysis was performed using two-way ANOVA. e, (left) Schematic of our proposed model of CAMP function in HR, c-NHEJ and TLS regulation. (right) The table showing summary of Olaparib and MMC sensitivity of indicated cells.

Fig 4. The REV7 binding activity of CAMP is not required for the CAMP chromosome alignment function

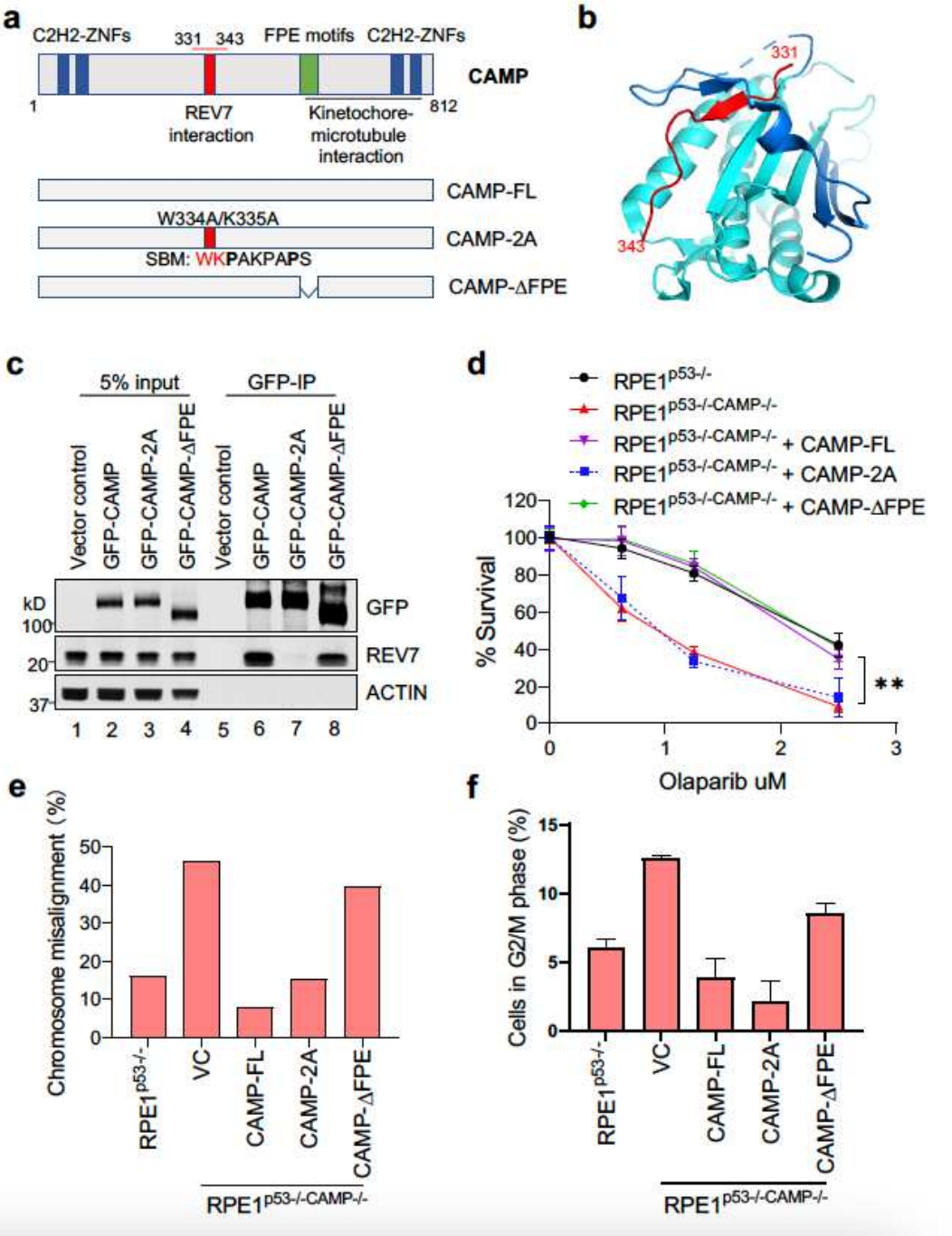

Figure 4

The REV7 binding region of CAMP is required for the HR function but not for correction of chromosome misalignment a, (Top) Schematic of CAMP protein showing its various domains and REV7 binding region. (Bottom) Schematic of CAMP-Full Length (FL) and two mutants (2A and ΔFPE). SBM, REV7 seatbelt binding motif. b, Structure of the REV7-CAMP complex. REV7 is shown in cyan and blue (seatbelt domain), and the CAMP fragment (residues 331-343) is shown in red. c, Western blot showing GFP-immunoprecipitation of GFP-Empty Vector, G 344 FP-CAMP wild-type, GFP CAMP-2A mutant or GFP-CAMP-ΔFPE, and the co-immunoprecipitation of endogenous REV7 in 293T cells. d, A 14 days clonogenic assay of indicated cell lines treated with various doses of Olaparib; n=3 independent experiments, **P<0.001. Statistical analysis was performed using two-way ANOVA. e, Summary of chromosome misalignment in indicated cell lines. f, Quantitative analysis of indicated cells in G2/M.

Fig 5. CAMP overexpression is common in tumors with underlying HR deficiency and correlates with poor cancer patient prognosis

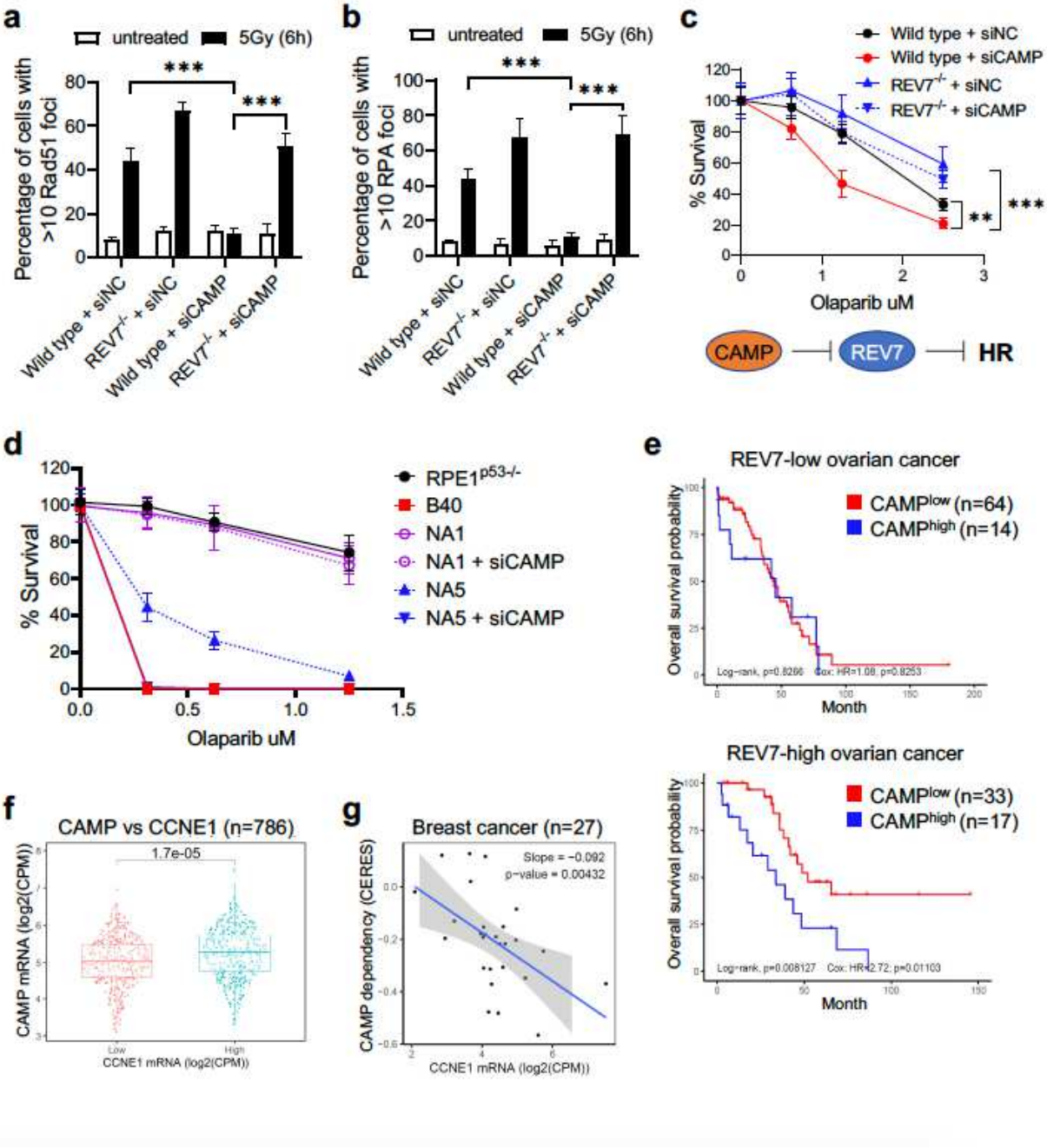

Figure 5

CAMP is epistatic to REV7 in the Regulation of Homologous Recombination Quantification of RAD51 (a) and p-RPA32(S33) (b) foci formation in wild-type and REV7-/- U2OS cells treated with siRNA negative control (siNC) and siCAMP, and 6 hours after 5Gy IR treatment.. More than 10 RAD51 foci were counted. n=3 biologically independent experiments, ***P < 0.0001. Statistical analysis was performed using two-tailed student's t-tests. c, A 14-days clonogenic survival of wild-type and REV7-/- U2OS cells treated with

various doses of Olaparib after siControl or siCAMP treatment. n=3 independent experiments, **P < 0.001, ***P < 0.0001. Statistical analysis was performed using two-way ANOVA. d, A 14-days clonogenic survival of RPE1p53-/-, RPE1p53-/-BRCA1-/- and niraparib/olaparib-resistant RPE1p53-/-BRCA1-/- cell clones treated with various doses of Olaparib after siControl or siCAMP treatment. n=3 independent experiments. Statistical analysis was performed using two-way ANOVA. e, Kaplan–Meier curves depicting overall survival of ovarian cancer patients with CAMP expression and REV7 expression. f, CAMP expression positively correlates with Cyclin E expression. g, Breast cancer cells with high expression of CCNE1 are more dependent on CAMP for survival.

Supplementary Files

This is a list of supplementary files associated with this preprint. Click to download.

- CAMPextendedfiguresfinal.pdf